Influence of Water on Carbon Dioxide and Room Temperature Ionic Liquid Dynamics: Supported Ionic Liquid Membrane vs. the Bulk Liquid

Jae Yoon Shin, Steven A. Yamada, and Michael D. Fayer*

Department of Chemistry,
Stanford University, Stanford, CA 94305

*Phone: 650 723-4446; Email: fayer@stanford.edu

Supporting Information

1. Experimental Methods for Time-resolved Ultrafast Infrared Experiments

A Ti:Sapphire regenerative amplifier pumps a home-built optical parametric amplifier creating mid-IR pulses centered at 2277 cm^{-1} with ~6 μJ pulse energy. An enclosure of the optical table was purged with H_2O and CO_2-scrubbed air to minimize atmospheric absorption. Because some CO_2 remained even with the purge, $^{13}CO_2$ that has its asymmetric stretch absorption shifted away from the $^{12}CO_2$ wavelength was used so that atmospheric $^{12}CO_2$ absorption did not affect the data.

The mid-IR beam was split into two beams, a stronger pump pulse and weaker probe pulse. The pump pulse was passed through an acousto-optic mid-IR Fourier-domain pulse-shaper. In the PSPP experiments, the pulse shaper chopped the pump pulse to obtain transient absorption signals, while in the 2D IR experiments the pulse shaper generated two excitation pulses, 1 and 2, and controlled the delay time (τ) between them. In addition, the pulse shaper controlled the phase of the pulses and was used to overcome light scattering that is the major difficulty in performing the laser experiments on highly scattering non-transparent membranes. A 4-shot phase cycling scheme [1] was used for the 2D IR experiments with perpendicular polarization configuration as well as for the PSPP. In the 2D IR measurements with parallel polarization configuration, in which the scattered light was a more serious problem, an 8-shot phase cycling and chopping scheme was utilized.[2] A mechanical delay stage in the probe pulse path controlled the time delay between the pump and probe pulses in the PSPP experiments or the time delay (waiting time, T_w) between the second excitation pulse 2 and the third excitation pulse 3 (probe pulse) in the 2D IR experiments. The pump and probe pulses were focused into the sample with a small crossing angle for both experiments. After passing through the sample, the probe pulse was directed into a spectrograph. The spectrograph disperses the probe pulse,

which was then detected in the frequency-domain by a 32-pixel HgCdTe (MCT) IR array detector. The 2D IR signal is collinear with the third pulse (probe pulse), which also acts as the local oscillator (LO) used for heterodyne detection of the signal.

In the PSPP measurements, the probe polarization was horizontal (in the plane of the optical table) and the pump polarization was at 45° with respect to the probe pulse. After the sample, a polarizer mounted in a computer controlled rotation stage alternately resolved the probe pulse at +45° (parallel to the pump) and –45° (perpendicular to the pump) relative to the incident polarization (horizontal). Since the response of the spectrograph grating is polarization-dependent, another horizontal polarizer was placed in front of the spectrometer's entrance slit to ensure that there is no bias in the detection of the polarizations. The collected probe signals parallel, $S_{\parallel}(t)$, and perpendicular, $S_{\perp}(t)$, to the pump were used to obtain the population relaxation $P(t)$ and the second Legendre polynomial orientational correlation function $C_2(t)$ using[3]

$$S_{\parallel}(t) = P(t)[1 + 0.8C_2(t)] \tag{S1}$$

$$S_{\perp}(t) = P(t)[1 - 0.4C_2(t)] \tag{S2}$$

From these, the population relaxation is given by

$$P(t) = \frac{1}{3}[S_{\parallel}(t) + 2S_{\perp}(t)] \tag{S3}$$

The anisotropy, $r(t)$, is the transition dipole orientational correlation function (the second Legendre polynomial correlation function, $C_2(t) = \langle P_2(\hat{\mu}(t) \cdot \hat{\mu}(0)) \rangle$), scaled to 0.4

$$r(t) = \frac{S_{\parallel}(t) - S_{\perp}(t)}{S_{\parallel}(t) + 2S_{\perp}(t)} = 0.4C_2(t) \tag{S4}$$

In the 2D IR vibrational echo experiments, three excitation pulses 1, 2, and 3 impinge on the sample with controllable time delays, τ (delay between 1 and 2 pulses) and T_w (delay between 2 and 3 pulses). In effect, pulses 1 and 2 label the initial frequencies of the $^{13}CO_2$ asymmetric stretch vibrational oscillators. After the system evolves during T_w, pulse 3 generates the vibrational echo signal, reading out the final frequencies of the vibrational oscillators. To carry out the polarization selective measurements, the polarization of both excitation pulses 1 and 2 was set to 0° and 90° relative to the probe polarization (horizontal) in the $\langle XXXX \rangle$ (parallel) and $\langle XXYY \rangle$ (perpendicular) configurations, respectively, using a polarizer and half-wave-plate. The

resolving polarizer after the sample is fixed to horizontal and is not changed for either polarization configurations. The 2D IR spectrum consists of the ω_m (vertical) and ω_τ (horizontal) axes and requires two Fourier transforms to obtain the frequency domain spectrum. The first Fourier transform yields the ω_m axis experimentally by resolving the frequencies of echo/LO pulse *via* the spectrograph, that is, the time domain pulse is taken into the frequency domain. Scanning τ in the experiments produces an interferogram at each ω_m because the echo signal moves in phase relative to the fixed in time LO. The numerical Fourier transform of this interferogram for each ω_m gives the ω_τ axis of the 2D IR spectrum.

For each T_w, a 2D IR spectrum is collected by scanning τ, and the spectral diffusion is evaluated based on the 2D line shape analysis at each T_w. The T_w dependent frequency-frequency correlation function (FFCF) contains the dynamical information of interest. The center line slope (CLS) method[4-5] was employed to obtain the normalized FFCF (CLS(T_w)) from the 2D IR spectra. A plot of the CLS vs T_w is the normalized T_w-dependent portion of the FFCF. Given the CLS(T_w) and the linear absorption spectrum, the full FFCF including the homogeneous component can be determined.

2. Second-order Stark Effect RISD Theory

It has recently been shown that the rotational motions of the probe molecule itself can contribute to the spectral diffusion along with the structural fluctuations of the medium.[6-8] The contribution to spectral diffusion from the orientational relaxation of the probe molecule is called reorientation induced spectral diffusion (RISD) while spectral diffusion from the structural fluctuations of the medium is called structural spectral diffusion (SSD). RISD and SSD for $^{13}CO_2$ in bulk EminNTf$_2$ has been described in complete detail.[6] For $^{13}CO_2$, RISD is caused by a second order Stark effect. When the $^{13}CO_2$ rotates in the electric field produced by the surrounding medium, the Stark coupling changes causing a shift in the vibrational frequency, i.e., RISD. RISD makes the CLS decay faster than it would if only SSD occurred. The RISD and SSD contributions can be separated using the independently measured anisotropy decay, which characterizes the rotational dynamics of the $^{13}CO_2$, and the CLS decays from polarization selective 2D IR experiments.[6, 9] The contribution of RISD differs in two polarization configurations, $\langle XXXX \rangle$ (parallel) and $\langle XXYY \rangle$ (perpendicular), causing the CLS decays to differ. $\langle XXXX \rangle$ means the polarizations of the three input pulses and the echo signal are all the

same. $\langle XXYY \rangle$ means the third pulse and the echo signal have polarizations that are perpendicular to the first and second pulses. The polarization of pulses 1 and 2 is set perpendicular to the third pulse, and the combined echo and LO are detected through a polarizer set to the *Y* polarization.

The second-order Stark effect RISD theory permits the total FFCF to be separated into SSD and RISD contribution, and a further separation of the SSD into contributions that result from scalar and vector interactions of the medium with the $^{13}CO_2$.[6, 9] Rotation of the probe will only affect the vector contributions to the FFCF. For a particular polarization configuration denoted as *p*, the polarization-weighted FFCF, $C_p(t)$, in the second-order Stark effect model is given by

$$C_p(t) = \langle \delta\omega(t)\delta\omega(0) \rangle_p = F_s(t) + F_v(t) R_p^{(2)}(t) \tag{S5}$$

where $F_s(t)$ is the correlation function of the scalar-coupled frequency fluctuations, and $F_v(t)$ is the correlation function of frequency fluctuations with vectorial coupling to the electric field. $R_p^{(2)}(t)$ is the RISD correlation function for second-order Stark coupling and given by[6]

$$R_{\langle XXXX \rangle}^{(2)}(t) = \frac{1}{175}\left[\frac{28 + 215C_2(t) + 72C_4(t)}{1 + 4/5C_2(t)}\right]$$

$$R_{\langle XXYY \rangle}^{(2)}(t) = \frac{1}{175}\left[\frac{-14 + 155C_2(t) - 36C_4(t)}{1 - 2/5C_2(t)}\right] \tag{S6}$$

$$R_{isotropic}^{(2)}(t) = C_2(t)$$

for the parallel, perpendicular, and isotropic configurations, respectively. In Equations S6, $C_2(t)$ and $C_4(t)$ are the second and fourth-order Legendre orientational correlation functions, respectively. $C_2(t)$ was experimentally determined from the anisotropy decays using the PSPP measurements. Once $C_2(t)$ is known, $C_4(t)$ can be calculated.[6-7] Then, the $R_p^{(2)}(t)$ are completely determined from the experimental anisotropy measurements. There are no adjustable parameters in these terms when they are used to fit the CLS data. The desired SSD parameters are obtained from fitting the CLS decay curves. The scalar and vector correlation terms, $F_s(t)$ and $F_v(t)$,

associated with SSD are the only free variables in the polarization-weighted FFCF (Equation S5).

3. Isotropic FFCF calculations

Although the polarization dependent CLS data permits the SSD part to be separated from total FFCF without the RISD contributions, theoretical calculations like the molecular dynamics (MD) simulations will determine the complete FFCF without a separation into SSD and RISD components.[10] An MD simulation generally does not include polarized E-fields of the excitation pulses. From the experiments, the isotropic configuration is obtained by taking the parallel 2D spectrum and adding 2 times the perpendicular spectrum with the spectra properly normalized. The resulting isotropic curve is, therefore, useful for the comparisons to the MD simulations. The isotropic decay still contains the RISD but it is not for a particular polarization configuration.

The FFCF is modeled with a multiexponential form

$$C(t) = \langle \delta\omega(t)\delta\omega(0) \rangle = \sum_i \Delta_i^2 \exp(-t/\tau_i) \tag{S7}$$

where Δ_i and τ_i are the frequency fluctuation amplitudes and associated time constants, respectively, for the *i*th component. $\delta\omega(t) = \omega(t) - \langle \omega \rangle$ is the instantaneous frequency fluctuation, where $\langle \omega \rangle$ is the average frequency. A component of the FFCF is motionally narrowed if $\Delta\tau < 1$, and then its Δ and τ cannot be determined separately. The motionally narrowed component contributes to the homogeneous broadening of the absorption line and has a pure dephasing linewidth, given by $\Gamma^* = \Delta^2\tau/\pi = 1/(\pi T_2^*)$, where T_2^* is the pure dephasing time. The vibrational lifetime and orientational relaxation also contribute to the homogeneous broadening through the total homogeneous dephasing time, T_2 which is given by

$$\frac{1}{T_2} = \frac{1}{T_2^*} + \frac{1}{2T_1} + \frac{1}{3T_{or}} \tag{S8}$$

where T_1 and T_{or} are the vibrational lifetime and orientational relaxation time, respectively. Then, the total homogeneous linewidth is $\Gamma = 1/(\pi T_2)$. As mentioned in Section 1, the FFCF can be extracted from the line shape analysis of 2D IR spectra, using the CLS method.[4-5] The isotropic FFCF parameters are obtained from the isotropic CLS decays are given in Table S2.

4. 2D IR CLS Decay Curves from Parallel Polarization Configuration

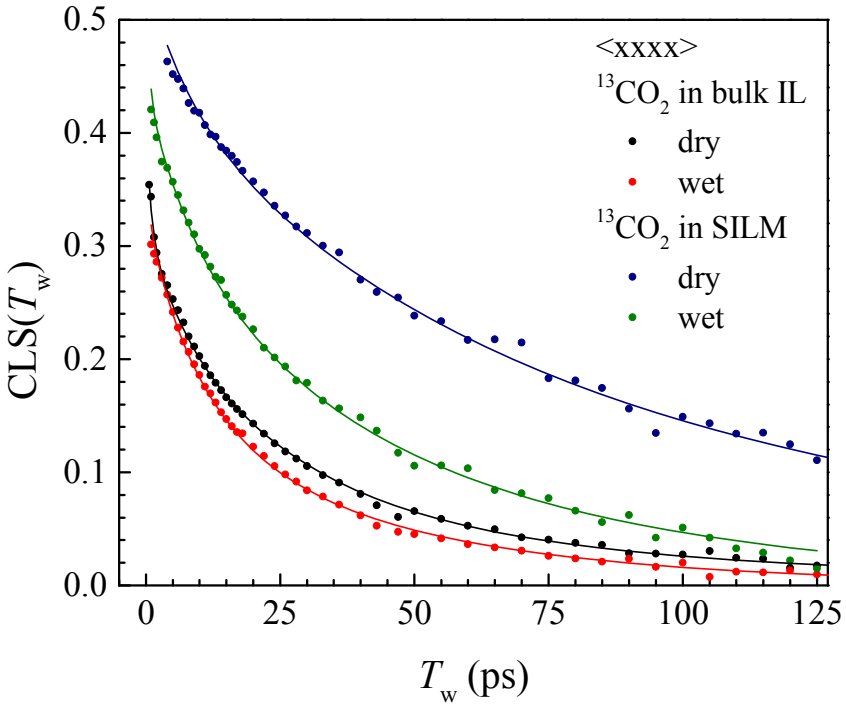

Figure S1. 2D IR CLS decay data of $^{13}CO_2$ in the bulk EmimNTf$_2$ and SILM from the parallel polarization configuration. The solid curves are the second-order RISD fits to the data. The data of dry samples were reproduced from ref [11].

Table S1. Triexponential fit parameters from the anisotropy data

Sample		A_1[a]	t_1 (ps)	A_2[a]	t_2 (ps)	A_3[a]	t_3 (ps)
Bulk	Dry	0.36 ± 0.02	0.9 ± 0.1	0.27 ± 0.01	6.7 ± 0.7	0.38 ± 0.01	52 ± 1
	Wet	0.48 ± 0.05	0.5 ± 0.1	0.21 ± 0.01	4.7 ± 0.6	0.31 ± 0.01	31 ± 1
SILM	Dry	0.38 ± 0.04	0.6 ± 0.1	0.22 ± 0.01	7.5 ± 0.9	0.40 ± 0.01	90 ± 2
	Wet	0.40 ± 0.03	0.5 ± 0.1	0.27 ± 0.01	7.5 ± 0.5	0.33 ± 0.01	84 ± 2

[a] A_i is the amplitude of each exponential for the normalized orientational correlation function.

Table S2. Isotropic FFCF parameters

Sample		Γ (cm^{-1})[a]	Δ_1 (cm^{-1})[b]	τ_1 (ps)[c]	Δ_2 (cm^{-1})[b]	τ_2 (ps)[c]
Bulk	Dry	3.0 ± 0.1	1.03 ± 0.02	7.2 ± 1.2	0.94 ± 0.06	52 ± 4
	Wet	3.1 ± 0.1	1.08 ± 0.02	9.0 ± 1.1	0.84 ± 0.05	47 ± 3
SILM	Dry	2.5 ± 0.2	0.92 ± 0.05	14.2 ± 1.9	1.2 ± 0.07	82 ± 12
	Wet	2.7 ± 0.2	1.1 ± 0.01	11.8 ± 3.0	1.0 ± 0.1	60 ± 7

[a] Γ: homogeneous line width (FWHM). [b] Δ_i: inhomogeneous line width (standard deviation) of the *i*th component. [c] τ_i: decay time constant of the *i*th component.

References

1. Kumar, S. K.; Tamimi, A.; Fayer, M. Comparisons of 2D IR Measured Spectral Diffusion in Rotating Frames Using Pulse Shaping and in the Stationary Frame Using the Standard Method. *J. Chem. Phys.* **2012,** *137* (18), 184201.

2. Nishida, J.; Tamimi, A.; Fei, H.; Pullen, S.; Ott, S.; Cohen, S. M.; Fayer, M. D. Structural Dynamics Inside a Functionalized Metal–Organic Framework Probed by Ultrafast 2D IR Spectroscopy. *Proc. Natl. Acad. Sci. U. S. A.* **2014,** *111* (52), 18442-18447.

3. Tokmakoff, A. Orientational Correlation Functions and Polarization Selectivity for Nonlinear Spectroscopy of Isotropic Media. I. Third Order. *J. Chem. Phys.* **1996,** *105* (1), 1-12.

4. Kwak, K.; Park, S.; Finkelstein, I. J.; Fayer, M. D. Frequency-Frequency Correlation Functions and Apodization in Two-Dimensional Infrared Vibrational Echo Spectroscopy: A New Approach. *J. Chem. Phys.* **2007,** *127* (12), 124503.

5. Kwak, K.; Rosenfeld, D. E.; Fayer, M. D. Taking Apart the Two-Dimensional Infrared Vibrational Echo Spectra: More Information and Elimination of Distortions. *J. Chem. Phys.* **2008,** *128* (20), 204505.

6. Giammanco, C. H.; Kramer, P. L.; Yamada, S. A.; Nishida, J.; Tamimi, A.; Fayer, M. D. Carbon Dioxide in an Ionic Liquid: Structural and Rotational Dynamics. *J. Chem. Phys.* **2016,** *144* (10), 104506.

7. Kramer, P. L.; Nishida, J.; Fayer, M. D. Separation of Experimental 2D IR Frequency-Frequency Correlation Functions into Structural and Reorientation-Induced Contributions. *J. Chem. Phys.* **2015,** *143* (12), 124505.

8. Kramer, P. L.; Nishida, J.; Giammanco, C. H.; Tamimi, A.; Fayer, M. D. Observation and Theory of Reorientation-Induced Spectral Diffusion in Polarization-Selective 2D IR Spectroscopy. *J. Chem. Phys.* **2015,** *142* (18), 184505.

9. Giammanco, C. H.; Yamada, S. A.; Kramer, P. L.; Tamimi, A.; Fayer, M. D. Structural and Rotational Dynamics of Carbon Dioxide in 1-Alkyl-3-methylimidazolium Bis(trifluoromethylsulfonyl)imide Ionic Liquids: The Effect of Chain Length. *J. Phys Chem. B* **2016,** *120* (27), 6698-6711.

10. Daly, C. A.; Berquist, E. J.; Brinzer, T.; Garrett-Roe, S.; Lambrecht, D. S.; Corcelli, S. A. Modeling Carbon Dioxide Vibrational Frequencies in Ionic Liquids: II. Spectroscopic Map. *J. Phys Chem. B* **2016,** *120* (49), 12633-12642.

11. Shin, J. Y.; Yamada, S. A.; Fayer, M. D. Carbon Dioxide in a Supported Ionic Liquid Membrane: Structural and Rotational Dynamics Measured with 2D IR and Pump–Probe Experiments. *J. Am. Chem. Soc.* **2017,** *139* (32), 11222-11232.